Cellular Oncology 27 (2005) 237–244
IOS Press

Multi-resolution wavelet-transformed image analysis of histological sections of breast carcinomas

Hae-Gil Hwang [a], Hyun-Ju Choi [a], Byeong-Il Lee [b], Hye-Kyoung Yoon [c], Sang-Hee Nam [d] and Heung-Kook Choi [a,*]

[a] *School of Computer Engineering, Inje University, Korea*
[b] *Department of Nuclear Medicine, Chonnam National University, Korea*
[c] *Department of Pathology, Inje University, Korea*
[d] *Medical Imaging Research Center, Inje University, Korea*

Abstract. Multi-resolution images of histological sections of breast cancer tissue were analyzed using texture features of Haar- and Daubechies transform wavelets. Tissue samples analyzed were from ductal regions of the breast and included benign ductal hyperplasia, ductal carcinoma *in situ* (DCIS), and invasive ductal carcinoma (CA). To assess the correlation between computerized image analysis and visual analysis by a pathologist, we created a two-step classification system based on feature extraction and classification. In the feature extraction step, we extracted texture features from wavelet-transformed images at 10× magnification. In the classification step, we applied two types of classifiers to the extracted features, namely a statistics-based multivariate (discriminant) analysis and a neural network. Using features from second-level Haar transform wavelet images in combination with discriminant analysis, we obtained classification accuracies of 96.67 and 87.78% for the training and testing set (90 images each), respectively. We conclude that the best classifier of carcinomas in histological sections of breast tissue are the texture features from the second-level Haar transform wavelet images used in a discriminant function.

Keywords: Multi-resolution, wavelet-transformed, breast cancer, texture features, statistics-based multivariate analysis, neural network

1. Introduction

Breast cancer is a malignancy that may develop into metastatic disease. The recent increase in the incidence of breast cancer among Korean women highlights the importance of studying breast cancer and its diagnosis [23]. Image analysis of tissue sections holds promise for diagnosing cancer and tracking disease progression. However, because conventional histological classification is based on subjective evaluations that are subject to both intra- and inter-observer variability, it is difficult to accurately reproduce descriptions of tissue texture [28]. Therefore, we have attempted to create a more uniform and highly reproducible classification system.

*Corresponding author: Prof. Heung-Kook Choi, Obang-dong 607, School of Computer Engineering, Inje University, Gimhae, Gyungnam, 621-749, Rep. of Korea. Tel.: +82 55 320 3437; Fax: +82 55 322 3107; E-mail: hkchoi@mitl.inje.ac.kr.

An optimal classifier for breast tumors requires the extraction from images of the relevant features that accurately describe the order/disorder of nuclear variation. Feature extraction is a particularly important step in the classification process, because the performance of the latter depends on the features extracted. Methods that classify tumors according to the presence of duct-forming cancer cells, pleomorphism of the nucleus, and mitotic cell division have proven useful for the post-mortem diagnosis of breast cancer [7,20,23, 32]. In addition, features describing the internal structure of cells (granularity and regularity of chromatin), irregularity of size and shape of the nucleus, and the distance between nuclei, are important for predicting disease progression [5,19,29].

Histology-based statistical analyses of textural features are frequently based on a gray level co-occurrence matrix (GLCM) [15,27]. Structural analysis methods describe the properties as well as the position of texture elements [16]. The spatial analysis of frequency

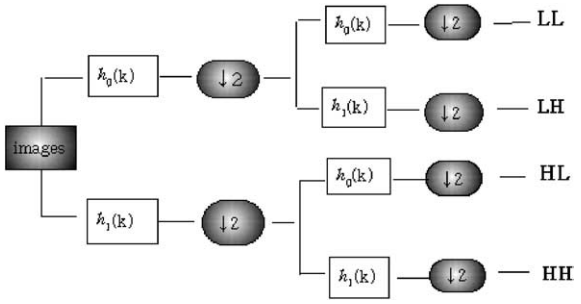

Fig. 1. Two-dimensional first-level wavelet decomposition.

information from images is best conducted in Fourier-transformed images [12], and further transformed by means of wavelet transforms [1,37].

Discrete wavelet transform is frequently used for signal processing, pattern recognition, and image processing. Wavelet transform is suitable for multi-resolution analysis as its basis is the decomposition of an image into a series of sub-sampled images of low resolution [3,8,24,38]. The wavelet transform uses a base function of translation and scaling that is applied to a nested set of multi-resolution images. Equation (1) shows the base function of the Haar transform in which a is a scaling variable, b is a translation variable, and ψ is the wavelet basis function (mother wavelet) [3]. Equation (2) shows the base function of the Daubechies transform in which h is a coefficient and ϕ is the scaling function [26].

$$\psi_{a,b}(t) = \frac{1}{\sqrt{2}}\psi\left(\frac{t-b}{a}\right), \tag{1}$$

$$\psi\left(\frac{t}{2}\right) = -h_3\phi(t+2) + h_2\phi(t+1) - h_1\phi(t) + h_0\phi(t-1). \tag{2}$$

To apply a wavelet transform to an image, the one-dimensional wavelet transform must be extended to the two-dimensional wavelet transform as illustrated (Fig. 1). A straightforward manner to achieve this is by filtering [35]. Specifically, the wavelet transform can be performed by applying a high-pass and low-pass filter sequentially along the rows and columns comprising the image.

The Haar transform is a relatively simple wavelet transform that decomposes a discrete signal into two sub-signals, each of which is half the extent of the original signal [3]. One sub-signal is a running average or trend, and the other is a running difference or fluctuation [38]. For example, the Haar transform (Fig. 2) can be described using scalar products with scaling and wavelets.

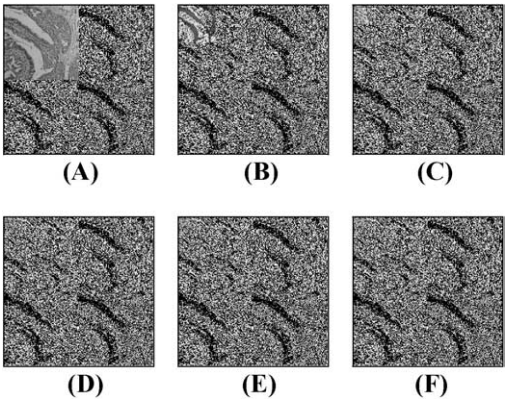

Fig. 2. Multilevel wavelet-transformed images of tissue carcinomas. Images in (A)–(F) correspond to levels 1–6.

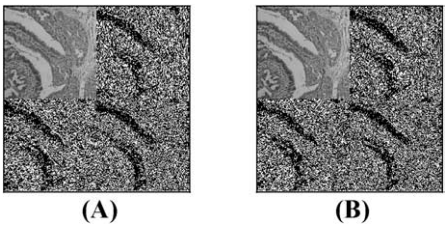

Fig. 3. Haar (A) and Daubechies (B) transform wavelet images (first level).

The Daubechies transform (Fig. 3B) is defined in essentially the same way as the Haar wavelet transform [24,26]. It uses the aforementioned relationships to construct orthonormal wavelets with compact support and a maximum number of vanishing moments. The Daubechies wavelet transform can be extended to multiple levels as many times as the signal length can be divided in half.

The Haar scaling functions are $\frac{1}{\sqrt{2}}$, $\frac{1}{\sqrt{2}}$, and the Haar wavelet coefficients are $\frac{1}{\sqrt{2}}$, $-\frac{1}{\sqrt{2}}$. The Daubechies scaling functions are $\frac{1+\sqrt{3}}{4\sqrt{2}}$, $\frac{3+\sqrt{3}}{4\sqrt{2}}$, $\frac{3-\sqrt{3}}{4\sqrt{2}}$, $\frac{1-\sqrt{3}}{4\sqrt{2}}$, and the Daubechies wavelet coefficients are $-\frac{1-\sqrt{3}}{4\sqrt{2}}$, $\frac{3-\sqrt{3}}{4\sqrt{2}}$, $-\frac{3+\sqrt{3}}{4\sqrt{2}}$, $\frac{1+\sqrt{3}}{4\sqrt{2}}$. A comparison of the two types of transform is shown (Fig. 3).

Multilevel wavelet transform has been shown to have a substantial effect on the accuracy of classification of prostate cancer of different grades when using texture features [18].

2. Materials and methods

We have evaluated the classification of lesions in histological sections of breast tissue using feature extraction, using Haar and Daubechies transform wavelets [24,26], in combination with two types of classification algorithms, i.e. discriminant analysis and a back-propagating neural network. Discriminant analysis is often used for classification purposes. It is descriptive in nature and facilitates the identification of boundaries between data that belong to different groups. When the prerequisites for discriminant analysis are met, this type of analysis produces linear combinations of discriminating variables that maximize the degree of separation among groups of data. Discriminant analysis has been used previously to classify breast carcinomas [31]. The second type of classifier was a back-propagating neural network, which was 'trained' to minimize the rate of classification errors

2.1. Tissue samples and image acquisition

Samples of breast tissue were obtained from breast cancer patients at Busan Paik Hospital, Inje University in Korea in 1999 and 2000. Samples included the following types of tissue: benign ductal hyperplasia, ductal carcinoma *in situ* (DCIS), and invasive ductal carcinoma (CA). After excision, tissue was fixed in 10% formalin and processed routinely for histology (Thermoeletron; Shandon, UK) before being embedded in paraffin wax. The embedded tissue was sectioned (4 μm). Tissue sections were deparaffinized, hydrated, and stained with hematoxylin and eosin (H&E) using an Autostainer XL (Leica, UK).

Digital images of the sections were acquired by a pathologist at a magnification of 10× with a 0.3 NA objective using a digital camera (Olympus C-3000) attached to a microscope (Olympus BX-51). Image resolution was 640 × 480 pixels and 24 bits per pixel. We collected a total of 180 images from 180 samples, 60 images for each type of tissue subdivided into 30 images for the training set and 30 images for the test set. A region of interest (ROI) of 256 × 256 pixels was selected from each digital image for the wavelet transform by a pathologist. To facilitate image processing red/green/blue (RGB) color images were converted into 8-bit gray levels using Eq. (3) [6].

$$Gray = Red \cdot 0.35 + Green \cdot 0.58 + Blue \cdot 0.07. \quad (3)$$

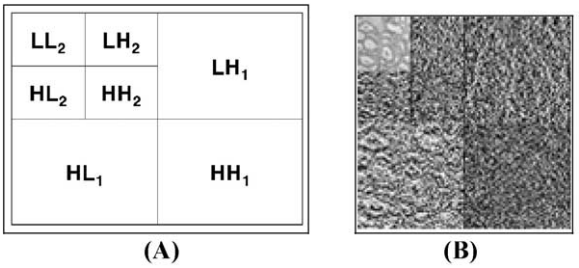

Fig. 4. Location of frequency bands in a sub-sampled image; (A) the second-level wavelet-transformed structure, (B) the applied a ductal carcinoma *in situ*.

2.2. Feature extraction

2.2.1. Wavelet transform

In the feature extraction step, we extracted texture features from Haar and Daubechies wavelet-transformed images [24,26]. To find a correlation between the rate of correct classification and wavelet depth, we applied one to six levels of wavelet transforms to the images and extracted texture features from the transformed images.

The wavelet transform reduced the image into four sub-sampled images: one high-pass filtered in both the horizontal and vertical direction (HH); one high-pass filtered in the vertical direction and low-pass filtered in the horizontal direction (HL); one low-pass filtered in the vertical direction and high-pass filtered in the horizontal direction (LH); and one low-pass filtered in both directions (LL) [3,35] (Fig. 4). We have artificially increased the intensity of the multilevel wavelet-transformed sub-sampled images, because the original texture description values are too low pixel intensity to visualize. The LL image was used as the input for the next level of the transform.

2.2.2. Extraction of texture features

After the sequential application of the wavelet transforms from one to six levels of images, we constructed a GLCM of the decomposed images at each level (depth). A low-resolution image was obtained by iteratively blurring the image, e.g., LL_2 (Fig. 4), and all the subsequent level wavelet transform LL_i images. The sub-sampled images could be found the texture information that was lost during the aforementioned processes.

From each GLCM, we calculated four texture features which were significantly discriminant out of a total of 21 texture features [25] from which we selected the significant features, namely entropy, energy, contrast, and homogeneity [4,15], as follows.

$$Entropy = -\sum_{i=0}^{N-1}\sum_{j=0}^{N-1}(PM)\log(PM),$$

$$Energy = \sum_{i=0}^{N-1}\sum_{j=0}^{N-1}PM^2,$$

$$Contrast = \sum_{i=0}^{N-1}\sum_{j=0}^{N-1}(i-j)^2PM,$$

$$Homogeneity = \sum_{i=0}^{N-1}\sum_{j=0}^{N-1}\left(1+(i-j)^2\right)^{-1}PM.$$

In the equations above, the co-occurrence probability matrix (PM) is constructed from the image by estimating the pairwise statistics of pixel intensity. Each element (i, j) of the matrix represents an estimate of the probability that two pixels with a distance have grey levels i and j. The distance, in this case, is specified by a displacement, d and an angle Θ. Therefore, the variance of the texture features due to image rotation was invariant. Each texture feature was extracted from each sub-sampled image.

2.3. Discriminant analysis

For the discriminant analysis of texture features of the transformed wavelet images, we used the discriminant analysis function available in the SAS software package (SAS Institute, NC, USA) [33]; cases were assumed to be independent. The texture feature data formed multivariate normal distributions within groups (e.g., for benign hyperplasia, DCIS, and CA tissue), and sometimes across groups [13].

2.4. Neural network

We used a standard back-propagation neural network algorithm that has been used previously [11,17, 30]. Our neural network was based on an unsupervised and error-correcting algorithm. The back-propagation algorithm used a multilayer perceptron and the generalized delta learning rule proposed by McClelland [21]. The multilayer perceptron network (MLP) was used to overcome the limitations of the perceptron. It comprised an input and an output layer, and at least one hidden layer. The back-propagation network was fully connected at each node for both feed-forward and backward propagation. The activation of the network proceeded in a single direction; specifically, activation proceeded from the input layer through the hidden layer to the output layer.

The back-propagation algorithm comprised two main steps: a feed-forward step in which the output of the nodes was computed, and a back-propagation step in which the weights were updated in an attempt to optimize agreement between the observed and desired output. The feed-forward step began at the input layer and worked forward to the output layer; the back-propagation step began at the output layer and worked backward to the input layer. In the present study, we cut off the minimal error level ($<10^{-5}$) for network training of the final matrix. The activation function for the hidden layer was the sigmoid function. Once training had been completed, the matrix was tested and validated. We used 16 (first level with 4 sub-samples), 28 (second level with 7 sub-samples), 40 (third level with 10 sub-samples), 52 (fourth level with 13 sub-samples), 64 (fifth level with 16 sub-samples), and 76 (sixth level with 19 sub-samples) input layer nodes. The four texture features in each sub-sample were calculated. There were 12 (first level), 19 (second level), 27 (third level), 35 (fourth level), 43 (fifth level), and 51 (sixth level) nodes in the hidden layer. The output layer always had three nodes. Each training set was presented to the network 100 times, which provided acceptable convergence.

3. Results

Representative images of tissue sections of the benign, DCIS, and CA tissue used in the current study are shown (Fig. 5). The color images in Fig. 5, part A, C and E are converted to 8-bit gray levels using Eq. (3).

The texture features that we extracted were entropy, energy, contrast, and homogeneity from 1–6 levels of the Haar and Daubechies wavelet-transformed images. For example, the Haar transform (Fig. 2) can be described using scalar products with scaling and wavelets. Figure 2, part A is applied the first level of the Haar transformed image and part F is applied the sixth level. Figure 3 is shown a comparison of the two types of transform, i.e., Harr and Daubechies transform. This transformed images visualized the implementation with Visual C++.

3.1. Classification of wavelets of levels 1 to 6

Classifiers were created from the texture features of the transformed wavelet images. In the training set that

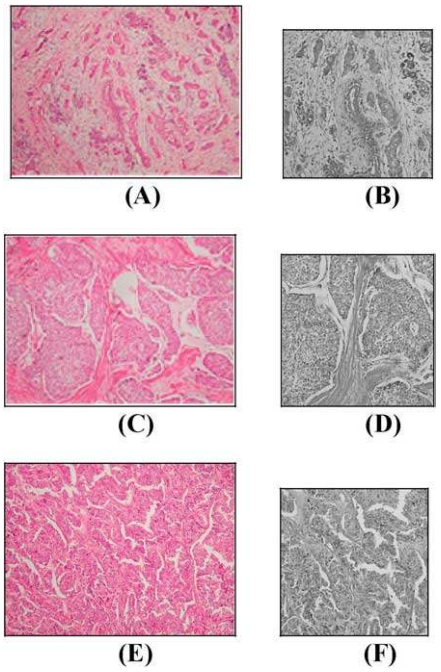

Fig. 5. Representative images of histological sections of breast tissue used in the present study (×10). (A,B) Benign hyperplasia. (C,D) Ductal carcinoma *in situ* (DCIS). (E,F) Invasive ductal carcinoma (CA). Images in (B), (D), and (F) correspond to randomly selected regions of interest (ROI) from (A), (C), and (E), respectively.

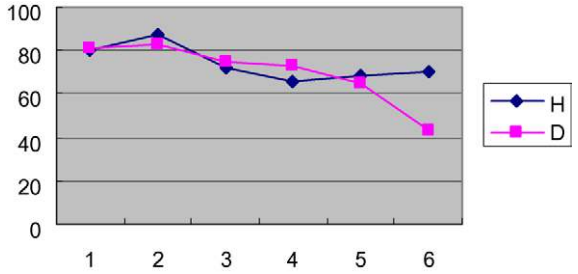

Fig. 6. Classification for levels 1–6 of 90 images of Haar (H) and Daubechies (D) transform wavelet images using discriminant analysis (X-axis: level; Y-axis: accuracy (%)).

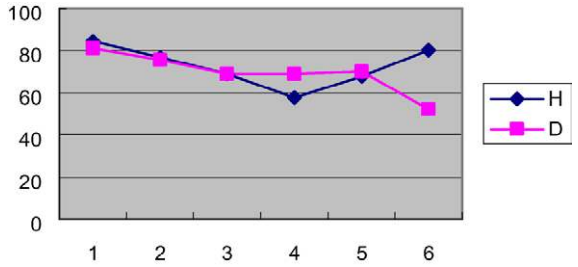

Fig. 7. Classification for levels 1–6 of 90 images of Haar (H) and Daubechies (D) transform wavelet images using a neural network (X-axis: level; Y-axis: accuracy (%)).

was used to train the network, we used 90 images (30 images of each type of tissue) to create two classifiers: the discriminant function statistic and the trained neural network. To find a correlation between the correct classification (i.e., the classification made by a pathologist) and the classifier for the various wavelet depths, we used 1 to 6 levels of wavelet-transformed images even though the wavelet transform is usually applied to only two or three levels. Image resolution was 256×256 pixels and 8 bits per pixel. The first-level wavelet transform was applied to the image which was divided into four sub-images (HH_1, HL_1, LH_1, LL_1) of 128 × 128 pixels each. The second-level sub-image of LL_1 was divided into four 64 × 64 pixel images, and so on until the sixth's-level sub-image (LL_6) which was divided into four 4 × 4 pixel images. 4 × 4 pixels is the minimum size used in GLCM. Finally, the image was subjected to the 6-level wavelet transform. The results of the classification based on the use of discriminant analysis and the neural network are presented in Tables 1 and 2, respectively.

The data in Tables 1 and 2 were used to construct the graphs depicted in Figs 6 and 7, respectively, to facilitate an evaluation of the two types of wavelet algorithms. Based on these graphs and the data in Tables 1 and 2, it was apparent that Haar wavelet features were relatively more stable than the Daubechies wavelet features.

3.2. The second-level Haar wavelet

The best classifier had a classification accuracy of 96.67% for the statistical multivariate classification using the second-level Haar transform wavelet image texture features in the training dataset, based on the test results. The confusion matrix for this classification result is shown in Table 3. The classifier thus identified was evaluated by applying it to the test set of 90 images, which resulted in a classification accuracy of 87.78%. The confusion matrix for this classification is presented in Table 4.

4. Discussion

Our results suggest that the combination of texture feature extraction and discriminant analysis produces the most accurate classification of breast carcinomas in histological tissue sections. In the present study, we

Table 1
Classification using discriminant analysis based on wavelet image features from level 1 to 6 of the wavelet transforms

Wavelet	Level					
	1	2	3	4	5	6
Haar						
Train	93.33	**96.67**	96.67	100.0	100.0	100.0
Test	80.00	**87.78**	72.22	65.56	68.89	68.89
Daube chies						
Train	90.00	94.44	97.78	98.89	100.0	100.0
Test	81.11	83.33	74.44	73.33	64.44	43.33

Table 2
Classification using a back-propagation neural network on wavelet image features from level 1 to 6 of the wavelet transforms

Wavelet	Level					
	1	2	3	4	5	6
Haar						
Train	**95.56**	95.56	94.44	94.44	86.67	93.33
Test	**84.44**	76.67	68.89	57.78	67.78	80.00
Daube chies						
Train	95.56	95.56	95.56	94.44	85.56	98.89
Test	81.11	75.56	68.89	68.89	70.00	52.22

Table 3
Most accurate classification using extracted texture features from the second-level Haar transform wavelet images for the 90 training set images

Comp.	Subj.			Total (%)
	Benign	DCIS*	CA**	
Benign	29	0	1	30 (96.67)
DCIS	1	28	1	30 (93.33)
CA	0	0	30	30 (100.0)
Total	30	28	32	90 (96.67)

*Ductal carcinoma *in situ*.

**Invasive ductal carcinoma.

Table 4
Most accurate classification using extracted texture features from the second-level Haar transform wavelet images for the 90 test set images

Comp.	Subj.			Total (%)
	Benign	DCIS*	CA**	
Benign	27	2	1	30 (90.00)
DCIS	6	23	1	30 (76.67)
CA	1	0	29	30 (96.67)
Total	34	25	31	90 (87.78)

*Texture features were: entropy, energy, contrast, and homogeneity.

**Columns: computer-based classification.

***Rows: subjective classification by a pathologist.

obtained a classification accuracy of 96.67 and 87.78% for the training set and the test set, respectively. The best classifier of histological sections of cancerous breast tissue were the texture features from the second-level Haar transform wavelet images collected at 10× magnification.

For feature extraction, all of the wavelet transformed sub-images were used (i.e., the image was not segmented). To evaluate the significance of the extracted features, we applied the multivariate analysis (MANOVA) using the SAS program package. MANOVA is the statistical analysis method that is used to assess whether datasets from different groups have different characteristics. For each MANOVA test, the P-value (<0.001) is found. Using discriminant analysis, we found that as the number of wavelet levels (depths) in the training set increased, the rate of correct classifications in the test set decreased, except for the second level. The results obtained by the use of a neural network in the present study suggest that the best classifier is the one based on texture features from the first-level Haar transform wavelet images; the remaining levels (up to level 6) produced poorer classification rates. It is worth noting that Wiltgen et al. [36] were able to satisfactorily use features based on the spectral properties of fourth-level Daubechies wavelet-transformed images to discriminate between common nevi and malignant melanomas in tissue sections.

Some researches have used whole-slide scanning images. Diamond et al. [9] presented the discrimination between stroma and prostate adenocarcinomas using the sum of variance texture features and a morphologic approach that had been applied to the classification of normal tissue and glandular tissue. Hamilton et al. [14] also used the co-occurrence matrix of colorectal mucosa for the calculation of texture features. The most powerful feature was the number of density pixels. However, they did not use any wavelet transform and their scans took a long time to process. Their processing time was around 5.5 hours and their method resulted in a lower correct classification rate than the one used in our study.

It should be emphasized that the neural network-based system used in our study required a substantial amount of time for processing of the training dataset. An additional factor that should be considered is that texture features are very sensitive to focus, even to the extent that some researchers have used the extraction of texture features as a criterion for focusing [10,22, 27]. It is difficult to envision how a standardized classification system might be established, given the substantial variability in (a) the methods that are used to stain tissue sections, (b) the techniques that are used for image acquisition, (c) the features of different types of normal tissue and cancer tissue, and (d) the subjectivity of evaluations associated with intra- and inter-observer variability [4]. Tinacci et al. [34] evaluated inter-observer reproducibility by comparing the degree of agreement between evaluations of cytological features in unprocessed tissue sections and digital images of the same sections.

In our study, discriminant analysis produced a better outcome than the neural network. A neural network is very sensitive which means that in some cases very good results are obtained. However, in other cases undesirable results are obtained. In general, neural networks are good at interpolation, but not so good at extrapolation as our results show [2].

In future studies, we will concentrate on developing novel texture features and finding an optimal wavelet filter for histological images. We believe that the proposed histopathological method of classification is useful as a diagnostic tool to identify breast tumors.

Acknowledgements

The authors gratefully acknowledge the support of the Medical Image Technology Laboratory (MITL) staff, in particular Dr. Won-Yong Chong for technical assistance with the wavelet transform method, as well as the Department of Pathology at Inje University Hospital. This study was supported by a grant from the Korea Health 21 R&D Project, Ministry of Health & Welfare, Republic of Korea (02-PJ1-PG3-20601-0003).

References

[1] A. Aldroubi and M. Unser, *Wavelets in Medicine and Biology*, CRC Press, 1996.

[2] R. Beale and T. Jackson, *Neural Computing an Introduction*, JW Arrowsmith Ltd., 1992.

[3] C.S. Burrus, R.A. Gopinath and H. Guo, *Introduction to Wavelets and Wavelet Transforms: A Primer*, Prentice-Hall, Inc., 1998.

[4] H.J. Choi and H.K. Choi, Classification of bladder carcinoma cell tissue sections by image analysis, in: *Proc. 5th Korea–Germany Joint Workshop Adv. Med. Image Process*, 2001, pp. 187–196.

[5] H.K. Choi, J. Vasko, E. Bengtsson, T. Jarkrans, P. Malmstrom, K. Wester and C. Busch, Grading of transitional cell bladder carcinoma by texture analysis of histological section, *Anal. Cell. Pathol.* **6** (1994), 327–343.

[6] H.K. Choi, Segmentation of immunohistochemical breast carcinoma images using ML classification, *J. Korea Multimedia Soc.* **4**(2) (2001), 108–115.

[7] L.W. Dalton, D.L. Page and W.D. Dupont, Histological grading of breast carcinoma: A reproducibility study, *Cancer* **73** (1994), 2765–2770.

[8] A.P. Dhawan, Y. Chitre, C. Kaiser-Bonasso and M. Moskowitz, Analysis of mammographic microcalcificaions using gray-level image structure features, *IEEE Trans. Bio-Med. Eng.* **15**(3) (1996), 246–259.

[9] J. Diamond, N.H. Anderson, P.H. Bartels, R. Montironi and P.W. Hamilton, The use of morphological characteristics and texture analysis in the identification of tissue composition in prostatic neoplasia, *Hum. Pathol.* **35**(9) (2004), 1121–1131.

[10] M.M. Galloway, Texture analysis using gray level run lengths, *Comput. Graph. Image Process.* **4** (1975), 172–179.

[11] E. Gose, R. Rohnsonbaugh and S. Jost, *Pattern Recognition and Image Analysis*, Prentice-Hall, 1996.

[12] G.H. Granlund and H. Knutsson, *Signal Processing for Computer Vision*, Kluwer Academic Publishers, 1995.

[13] R.A. Johnson and D.W. Wichern, *Applied Multivariate Statistical Analysis*, Prentice-Hall Inc., 1998.

[14] P.W. Hamilton, P.H. Bartels, D. Thompson, N. Anderson, R. Montironi and J.M. Sloan, Automatic detection of dysplastic fields in colorectal tissue using image texture analysis, *J. Pathol.* **182** (1997), 68–75.

[15] R.M. Haralick, K. Shanmugam and I. Dinstein, Texture feature for image classification, *IEEE Trans. on System, Man, and Cybernetics*, **3**(6) (1973), 610–624.

[16] R.M. Haralick, Statistical and structural approaches to texture, *Proc. IEEE* **67**(5) (1979), 768–804.

[17] Y. Hayashi, R. Setiono and K. Yoshida, A comparison between two neural network rule extraction techniques for the diagnosis of hepatobiliary disorders, *Artif. Intell. Med.* **20** (2000), 205–216.

[18] K.J. Khouzani and H. Soltanian, Multiwavelet grading of pathological images of prostate, *IEEE Trans. Bio-Med. Eng.* **50**(6) (2003), 697–704.

[19] D.S. Kim and S.J. Lee, Diagnostic pathology of the breast, *Academia* (1990), 139–172.

[20] P. Kronqvist, T. Kuopio and Y. Collan, Effect of freezing on histologic grading of invasive ductal breast cancer, *Analyt. Quant. Cytol. Histol.* **25** (2003), 47–52.

[21] T.L. McClelland and D.E. Rumelhart, *Parallel Distributed Processing*, MIT Press and the PDP Research Group, Cambridge, 1986.

[22] B. Palcic, B. Jaggi and C. MacAulay, The importance of image quality for computing texture features in biomedical specimens, *Proc. SPIE* **1205** (1990), 155–162.

[23] C.I. Park, H.S. Koo and G.Y. Choi, The Korean society of pathologists, *Pathology*, 4th edn, Go moon sa, 2000.

[24] L. Prasad and S.S. Iyengar, *Wavelet Analysis with Application to Images Processing*, CRC Press, 1997.

[25] N.J. Pressman, Markovian analysis of cervical cell images, *J. Histochem. Cytochem.* **24** (1976), 138–144.

[26] R.M. Rao and A.S. Bopardikar, *Wavelet Transforms*, Addison-Wesley, 1998.

[27] K. Rodenacker, Invariance of texture features in image cytometry under variation of size and pixel magnitude, *Anal. Cell. Pathol.* **8** (1995), 117–133.

[28] K. Rodenacker and E. Bengtsson, A feature set for cytometry on digitized microscopic images, *Anal. Cell. Pathol.* **25** (2003), 1–36.

[29] H. Schulerud, G.B. Kristensen, K. Liestol, L. Vlatkovic, A. Reith, F. Albregtsen and H.E. Danielsen, A review of caveats in statistical nuclear image analysis, *Anal. Cell. Pathol.* **16** (1998), 327–343.

[30] A.J.C. Sharkey, N.E. Sharkey and S.S. Cross, Adapting an ensemble approach for the diagnosis of breast cancer, *Proc. ICANN* (1998), 281–286.

[31] V. Sharifi-Salamatian, A.R. Roquancourt and J.P. Rigaut, Breast carcinoma, intratumour heterogeneity and histological grading, using geostatistics, *Anal. Cell. Pathol.* **20** (2000), 83–91.

[32] J.F. Simpson and D.L. Page, Status of breast cancer prognostication based on histopathologic data, *Am. J. Clin. Pathol.* **102** (1994), 3–8.

[33] Statistical Analysis System (SAS), 8.01, SAS Institute Inc. Cary, NC, USA, 2001.

[34] G. Tinacci, M.P. Cariaggi, F. Carozzi, A. Foggi, G. Miccinesi, F. Mirri, P. Pasquini, M. Zappa and M. Confortini, Digital images for interobserver variability comparison in cervicovaginal cytology, *Analyt. Quant. Cytol. Histol.* **25** (2003), 1–7.

[35] M. Vetterli and J. Kovacevic, *Wavelets and Subband Coding*, Prentice Hall, Inc., 1995.

[36] M. Wiltgen, A. Gerger, C. Wagner, P. Bergthaler and J. Smolle, Discrimination of benign common nevi from malignant melanoma lesions by use of features based on spectral properties of the wavelet transform, *Analyt. Quant. Cytol. Histol.* **25** (2003), 243–253.

[37] G.V. de Wouwer, P. Scheunders, S. Livens and D. Van Dyck, Wavelet correlation signatures for color texture characterization, *Pattern Recogn*. **32** (1999), 443–451.

[38] J.S. Walker, *A Primer on Wavelets and Their Scientific Applications*, CRC Press, LLC, 1999.